frontiers in Earth Science

ORIGINAL RESEARCH
published: 07 February 2020
doi: 10.3389/feart.2019.00359

South America Climate During the 1970–2001 Pacific Decadal Oscillation Phases Based on Different Reanalysis Datasets

Maria Elisa Siqueira Silva[1], Carlos Batista Silva[1]*, Tercio Ambrizzi[2], Anita Drumond[3] and Natália Nunes Patucci[1]*

[1] Department of Geography, Faculty of Philosophy, Letters and Human Sciences, University of São Paulo, São Paulo, Brazil, [2] Department of Atmospheric Sciences, Institute of Astronomy, Geophysics and Atmospheric Sciences, University of São Paulo, São Paulo, Brazil, [3] Institute of Environmental, Chemical and Pharmaceutical Sciences, Federal University of São Paulo, Diadema, Brazil

In this paper, circulation and precipitation climate patterns over the South American domain obtained from NCEP-NCAR reanalysis I, JRA-55, and ERA-40 reanalysis datasets were intercompared within the period 1970–2001 in order to verify their climatic association with the Pacific Decadal Oscillation, PDO. Although all three datasets showed similar climatic patterns during each PDO phase, they showed distinct intensities for circulation and precipitation variables. The mean low frequency flow propagation over the South Pacific during negative and positive PDO phases reached central-eastern South America with opposite signals, contributing to the modulation of the local climate. During the negative PDO phases, the northerly flow over South America is intensified, while during the positive phase it is weakened. NCEP-NCAR reanalysis I, in comparison with JRA-55 and ERA-40 values, always indicates the strongest signal for circulation and precipitation variables. NCEP-NCAR reanalysis I meridional wind at the low-level jet area was about 5 and 12% larger than the respective JRA-55 and the ERA-40 values. For the positive and negative PDO phases, only NCEP-NCAR and ERA-40 high-level zonal wind anomalies showed divergent (positive PDO) and convergent (negative PDO) patterns close to 140° W at equatorial latitudes of the Pacific Ocean, respectively. This one indicated distinct representations of the positioning of Walker cells in the three reanalysis datasets. GPCC dataset, NCEP-NCAR, JRA-55, and ERA-40 reanalysis showed, in general, the dipole precipitation pattern over eastern South America, with signs of changes between the central-eastern and southeastern areas during PDO reversal phases. Over the central-eastern South American region, NCEP-NCAR precipitation is, on average, 57% larger than GPCC values, and 35 and 46% larger than JRA-55 and ERA-40 values, respectively. The observed patterns of anomalies for different PDO phases appeared in all reanalysis datasets, leading us to conclude that the physical meaning is independent from the datasets. Even considering the JRA-55 climate signal over South America associated with the PDO influence as the weakest one, the ability of JRA-55 to calculate monthly precipitation provided the highest linear correlation coefficient values in tropical areas, leading us to consider this dataset as the most reliable for the studied area.

Keywords: South America climate, PDO, NCEP-NCAR I, JRA-55, ERA-40, GPCC

OPEN ACCESS

Edited by:
Wen Chen,
Institute of Atmospheric Physics (CAS), China

Reviewed by:
Maoqiu Jian,
Sun Yat-sen University, China
Eduardo Zorita,
Helmholtz Centre for Materials and Coastal Research (HZG), Germany

****Correspondence:***
Carlos Batista Silva
krlosbatist@gmail.com
Maria Elisa Siqueira Silva
elisasiq@usp.br

Specialty section:
This article was submitted to Atmospheric Science, a section of the journal Frontiers in Earth Science

Received: *02 August 2019*
Accepted: *30 December 2019*
Published: *07 February 2020*

Citation:
Silva MES, Silva CB, Ambrizzi T, Drumond A and Patucci NN (2020) South America Climate During the 1970–2001 Pacific Decadal Oscillation Phases Based on Different Reanalysis Datasets. Front. Earth Sci. 7:359. doi: 10.3389/feart.2019.00359

INTRODUCTION

Oceanic changes over the Pacific Ocean are potential inductors of the South American climate. Besides climate anomalies reached from convective variations over the tropical Atlantic and Pacific oceans, many studies have been carried out, indicating the low frequency propagation over the South Pacific and its perturbation of the South American climate on distinct scales (Mo and White, 1985; Mo and Ghil, 1987; Karoly, 1989; Mo and Higgins, 1998; Mo and Paegle, 2001; Grimm and Ambrizzi, 2009). One of the first studies considering low-frequency circulation patterns between the Southern Hemispheric middle and high latitudes was originally developed by Mo and White (1985). Later on, this pattern was well-described in Mo and Ghil (1987), and it was associated with quasi-stationary modes in the Southern Hemisphere, and characterized by wavetrains extending from central equatorial Pacific areas to the South American continent, known as the Pacific–South America (PSA) pattern. Before their contribution, other studies on the patterns of the low-frequency circulation characterization over the Northern Hemisphere (PNA patterns) were developed (Horel, 1981; Hoskins and Karoly, 1981; Wallace and Gutzler, 1981). In addition, a better understanding of quasi-stationary patterns between middle and high latitudes in the Northern Hemisphere and teleconnections patterns (Wallace and Gutzler, 1981) associated with the role of tropical heat sources (Walker and Bliss, 1932; Bjerknes, 1969) were developed. The role of heat sources on South American low-frequency circulation patterns was shown by Karoly (1989), completing the results of Mo and Ghil (1987), which showed the characteristic quasi-stationary pattern over South America.

Karoly (1989) showed the presence of low-frequency wavetrains throughout the South Pacific Ocean based on geopotential height data for three El Niño events (1972, 1976–1977, and 1982). Based on a barotropic model, Hoskins and Ambrizzi (1993) showed a building up of wavetrain guides due to heat sources around the world and some in particular that developed over the South Pacific due to the equatorial Pacific heating sources. Kidson (1999) and Mo (2000) also described the characteristic low-frequency wavetrain propagation pattern over the South Pacific and the Pacific-South America pattern. Mo and Higgins (1998) and Mo and Paegle (2001) depicted the importance of Pacific–South America 1, PSA1, and Pacific–South America 2, PSA2, the first modes of Empirical Orthogonal Functions (EOF) applied to wind data.

Mo and Paegle (2001) related the PSA1 mode to sea surface temperature (SST) over western equatorial Pacific areas, linking it to El Niño-South Oscillation (ENSO) variability. The PSA2 mode was associated by the authors with a 30- to 60-day Madden- Julian oscillation (Renwick and Revell, 1999). Silva et al. (2016) identified similar PSA patterns for distinct Pacific Decadal Oscillation (PDO) phases between 1970 and 2003, as in Mo and Higgins (1998), indicating the association between low-frequency oscillation through the South Pacific and preferred circulation patterns over South America. More recent contributions related to the role of PSA1 and PSA2 modes were associated with possible alterations in the extratropical Antarctic circulation (Nicolas and Bromwich, 2014; Irving and Simmonds, 2016).

Focusing on the decadal scale of precipitation variability, other studies have indicated the association between the South American climate and Pacific Decadal Oscillation (i.e., Villamayor et al., 2018 and references therein). PDO is characterized by SST anomaly decadal oscillation between equatorial and extratropical areas over the whole Pacific basin, influencing climatic patterns over many areas of the globe (Mantua and Hare, 2002), particularly over South America. Both Villamayor et al. (2018) and Kayano and Andreoli (2004) focused their studies on PDO climatic impact on northern South America. During positive SST anomalies over the equatorial Pacific, when the positive PDO phase is characterized, Villamayor et al. (2018) observed in general a negative precipitation anomaly over northern South America for the simulated CMIP5 (Climate Modeling Intercomparing Project, Taylor et al., 2012) data, associating it with subsident anomalies. Kayano and Andreoli (2004) suggested that decadal rainfall variability over northern northeast Brazil (1871–1991) might be independently related to decadal variability of PDO and South and North Tropical Decadal oscillations. Robertson and Mechoso (2000) associated precipitation and river streamflow increase over southeastern South American areas and the southeastern Amazonian region with positive PDO phases from 1978 to 1996. Marengo et al. (2004) showed a precipitation decrease over the northern Amazonian region after 1976–1977, also associating it with the PDO positive phase. Climatic impact over the whole South American domain related to PDO variability, comprising one positive and two negative PDO phases, was investigated for the first time by Silva et al. (2016). They identified the riverflow increase and decrease over the Pantanal region (seasonally-swamped lowlands in the central part of South America) with distinct positive and negative PDO phases during the period 1970–2001, respectively, associating it with different low-frequency circulation patterns throughout the South Pacific during reversed PDO phases.

To evaluate whether the findings by Silva et al. (2016) are not data dependent, the purpose of the present study is to analyze the circulation patterns over the Pacific and South America during reversal PDO phases observed between 1970 and 2001 provided by three distinct reanalysis datasets—the JRA-55 (Japanese Reanalysis (Kobayashi et al., 2015), the ECMWF ERA-40 (European Center for Medium-Range Weather Forecasts) (Uppala et al., 2005), and the NCEP-NCAR I (National Centre for Environment Prediction-National Centre for Atmospheric Research) (Kalnay et al., 1996)—focusing on the impacts over Southeastern Brazil.

DATA AND METHODS

Monthly wind, geopotential height, and precipitation data from January 1970 to December 2001 were considered in the present study. The reanalysis datasets considered were NCEP-NCAR reanalysis I, JRA-55, and ERA-40. The criteria considered for the dataset selection, ERA-40 and JRA-55, were the size of the time series, which covers the 1970–2001 period, and their quality. Besides ERA-40 and JRA-55 datasets, other reanalysis datasets were previously verified as possible in this comparative study, ERA-20C (Hersbach et al., 2015) and ERA-Interim (Dee et al.,

2011). ERA-20C in particular showed very distinct circulation patterns in relation to the NCEP-NCAR reanalysis, which made us discard it. Further studies must be developed to understand these differences. Since ERA-Interim starts in 1979, not covering the period of analysis, it was also discarded.

Harada et al. (2016) showed the evolution of the global Japanese reanalysis in relation to the previous one, JRA-25, and in relation to other reanalysis datasets, particularly the ERA-40 and the NCEP-NCAR reanalysis I. The application of more proper data assimilation systems (DAS), throughout the time period, provided better reanalysis datasets, mainly for tropical precipitation. Application of the four-dimensional variational analysis (4D-Var) (DAS 3rd generation) in the data assimilation system of JRA-55 led to a reduction in the dry bias over the Amazon basin and a higher temporal consistency of the temperature analysis (Harada et al., 2016). In relation to the Tropical Rainfall Measuring Mission data (TRMM) (Huffman et al., 2007; Harada et al., 2016) showed correlation mean values of JRA-55 tropical precipitation as good as that provided by MERRA reanalysis (Rienecker et al., 2011) and better values in relation to the ERA-40 reanalysis. The ERA-40 reanalysis was obtained by applying the 3D-Var technique (DAS 2nd generation) to the data assimilation system.

JRA-55 and ERA-40 datasets were compared with results obtained by Silva et al. (2016) who used NCEP-NCAR reanalysis I to describe the climate patterns over South America associated with the three PDO phases during the 1970–2001 period. Since ERA-40 reanalysis ranges from 1957 to 2001, all the computations were made for the period until 2001. Besides the precipitation from the reanalysis datasets, precipitation data from the Global Precipitation Climatology Centre (GPCC), which is considered a good estimate over continental areas (Schneider et al., 2008), were also used. The datasets used have the following spatial resolution: NCEP-NCAR, 2.5 degrees; JRA-55, 1.25 degrees; and ERA-40 and GPCC precipitation data (Adler et al., 2003), 1 degree. The monthly PDO index was obtained from NOAA (http://www.esrl.noaa.gov/psd/data/climateindices/list/). The PDO index is defined as the leading Empirical Orthogonal Function (EOF) mode of monthly SST anomalies in the North Pacific Ocean, poleward of 20°N (Mantua et al., 1997; Mantua and Hare, 2002; Mochizuki et al., 2010; Krishnamurthy and Krishnamurthy, 2014).

In order to retain low frequency oscillation (>1 year), and, thus, Rossby wave propagation, geopotential height and wind components for all three reanalysis datasets were smoothened with a Lanczos low-pass filter (Duchon, 1979). Following the analysis of Silva et al. (2016) and many other authors (Latif and Barnett, 1994, 1996; Hare and Francis, 1995; Mantua et al., 1997; Minobe, 1997; Zhang et al., 1997; Gershunov and Barnett, 1998; Mantua and Hare, 2002), the present study also considers three PDO phases between 1970 and 2001 defined by three subperiods: 1970–1976 (negative phase), 1977–1996 (positive phase), and 1997–2001 (negative phase). The climatic patterns associated with these three PDO phases were analyzed through mean maps, and the respective statistical significance was computed through a *t*-Student test. When the mean was computed for non-filtered data, the number of months in each subperiod (84, 240, and 60) was considered in the *t*-Student test; otherwise, the number of years was used (7, 20, and 5). Besides the South America climatic patterns in each PDO phase, low-frequency wave propagation from the equatorial Pacific to South America was identified. Before all the analyses (except the linear correlation) were made, the linear trend and seasonality based on the monthly climatology were removed from the original time series.

RESULTS

Circulation and precipitation data from NCEP-NCAR, ERA-40, and the JRA-55 reanalysis are compared in each PDO phase, allowing the identification of possible differences in the South American climate during the PDO phases between these three datasets. Mean maps for each one of the three PDO phases, 1970–1976, 1977–1996, and 1997–2001, which were respectively characterized as negative, positive, and negative phases, were analyzed.

Circulation Analysis

The mean atmospheric pattern associated with each PDO phase can be illustrated by filtered 250 hPa geopotential height data as shown in **Figure 1**. The three considered datasets, NCEP-NCAR, JRA-55, and the ERA-40 reanalysis, indicated similar low-frequency patterns between equatorial Pacific areas and the South American subtropical region for the three PDO phases, 1970–1976, 1977–1996, and 1997–2001. **Figures 1A,D,G** are similar to Figure 9 in Silva et al. (2016), which used only the NCEP-NCAR reanalysis I dataset. All the three datasets feature opposite anomalies for positive and negative PDO phases. During negative phases, 1970–1976 and 1997–2001 (1st and 3rd subperiods, 1st and 3rd columns in **Figure 1**), there were negative 250 hPa-geopotential height anomalies over the central equatorial Pacific associated with oceanic and atmospheric cooling in these periods, both in the Southern and Northern Hemispheres (though analyzed, SST and air temperature maps are not shown here) and positive 250 hPa-geopotential height anomalies over central-eastern South America, particularly over the southeast of Brazil. During the positive PDO phase (2nd subperiod, 1977–1996), an opposite pattern was observed in these three datasets, characterized by positive 250 hPa-geopotential height anomalies over the central equatorial Pacific (with the associated SST increasing over this area) and negative anomalies over central-eastern South America. We also notice in **Figure 1** wavetrains patterns of low frequency associated with Rossby waves in negative and positive PDO phases throughout the South Pacific, characterizing the Pacific-South America (PSA) pattern in a manner similar to that presented by previous studies (e.g., Mo and Ghil, 1987; Karoly, 1989; Mo and Paegle, 2001; Ding et al., 2011; Irving and Simmonds, 2016) obtained through EOF analysis. Although the three reanalysis datasets showed similar signal patterns for the three PDO periods, the geopotential height intensities featured some distinctions. It was noticed that the NCEP-NCAR data had the strongest anomalies in comparison to JRA- 55 and the ERA-40 reanalysis (**Figure 1**) for the negative

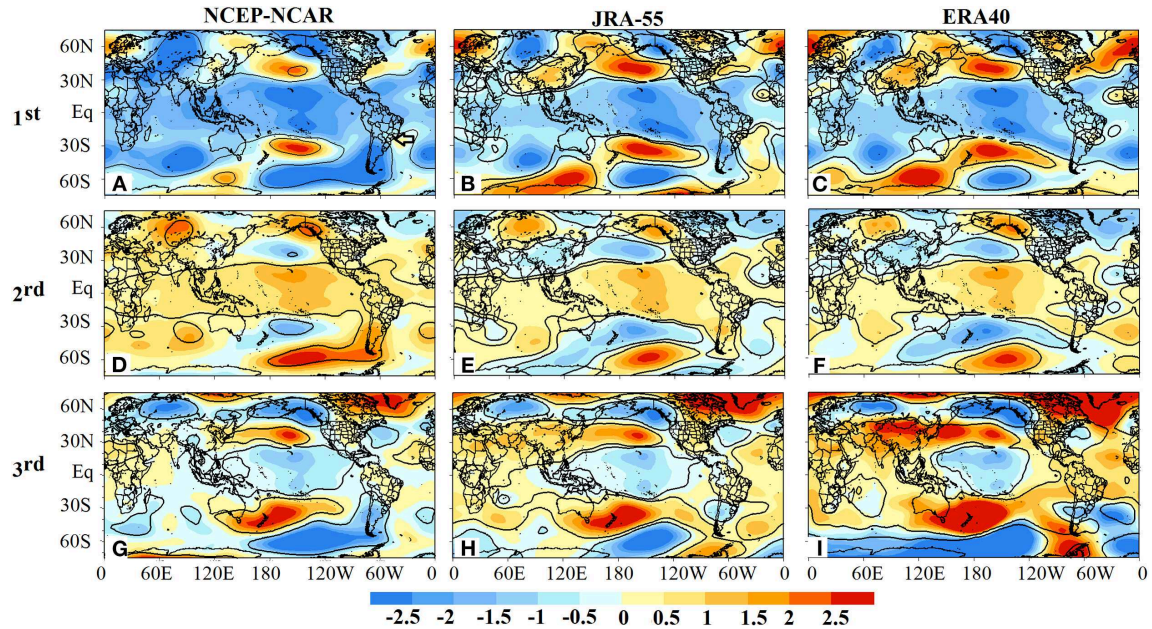

FIGURE 1 | Mean anomaly of filtered 250 hPa-geopotencial height (m^2 s^{-1}) for the **(A–C)** 1st, **(D–F)**, 2nd **(G–I)**, and 3rd subperiods for NCEP-NCAR **(A,D,G)**, JRA-55 **(B,E,H)**, and ERA-40 **(C,F,I)** reanalysis. Significant values for $\alpha = 0.05$ (*t*-Student test) are surrounded by black isolines.

and positive PDO phases, which are also related to stronger and weaker SST anomalies over the Pacific Ocean (figures not shown). Even over the Pacific Ocean, the 3rd subperiod presented a warmer mean troposphere when compared with the 1st subperiod (maps from NCEP-NCAR reanalysis I are not shown), although both were considered negative PDO phases in the entire 1970–2001 period, suggesting a possible climatic change response. This aspect must be investigated in further studies with longer time series, such as the ERA20C data (Poli et al., 2013, 2016).

In general, 250 hPa-geopotential height anomalies for the 2nd subperiod presented smaller absolute anomaly values (**Figures 1B,E,H**) than that for the 1st and 3rd subperiods (**Figures 1A,C,D,F,G,I**), possibly related to the length of each subperiod. The 2nd subperiod was 20 years, while the 1st and 3rd subperiods were 6 and 5 years, respectively. Although the number of years in the negative PDO phases, the 1st and 3rd, were lower—−5 and 6 years, respectively—than the positive PDO phase, the yearly analysis of geopotential height anomalies, not shown here, exhibited the same patterns for negative and positive PDO phases in almost all years, suggesting that the anomalous mean patterns computed for the negative PDO phases were not influenced by the difference in the length of the time series. The three datasets present similar spatial patterns and convergent results, showing opposite low-frequency propagation patterns between the equatorial Pacific and central-eastern South America during reversal PDO phases. Although the southeast of Brazil does not always show statistically significant values for geopotential height anomalies for all subperiods and datasets, it is a region of interest in this study. The importance of southeastern Brazil, besides being a highly populated area, is the fact that it is also the richest Brazilian economic region, with considerable agriculture, industrial production, and a strong third sector. Therefore, the analysis to be presented further on will sometimes focus on this area.

The 250 hPa-geopotential height anomalies of the 3rd subperiod show certain distinct patterns between the three reanalysis datasets. Besides anomalous wave propagation from the equatorial Pacific to the South Pacific being quite similar in the three reanalysis datasets (**Figures 1C,F,I**), spatial patterns over South America are distinct, particularly in the 3rd subperiod. NCEP-NCAR reanalysis I showed negative anomalies in a large part of southern South America in the 3rd subperiod, while the JRA-55 and ERA-40 geopotential height anomalies presented positive signs. Even so, over southeastern Brazil there was in general a close agreement between these three datasets. In terms of differences between reanalysis data, this region showed inverted patterns of 250 hPa-geopotential height during the opposite PDO phases for the three datasets, which means that there was some agreement between overall patterns provided by the different datasets.

During negative PDO phases (1st and 3rd subperiods), the central-eastern South America region delimited by the 60–40°W and 25–15°S coordinates, including the Brazilian southeastern area, presented positive geopotential height anomaly at high levels in the three datasets (**Figures 1A,C,D,F,G,I**, respectively, for NCEP-NCAR I, JRA-55, and ERA-40 datasets). Conversely, during the positive PDO phase (2nd subperiod), the same area presented negative mean geopotential height anomalies (**Figures 1D–F**). Patterns characterized by positive (negative) geopotential height anomalies at high levels over southeastern Brazil may be associated with dry and divergent (moist and

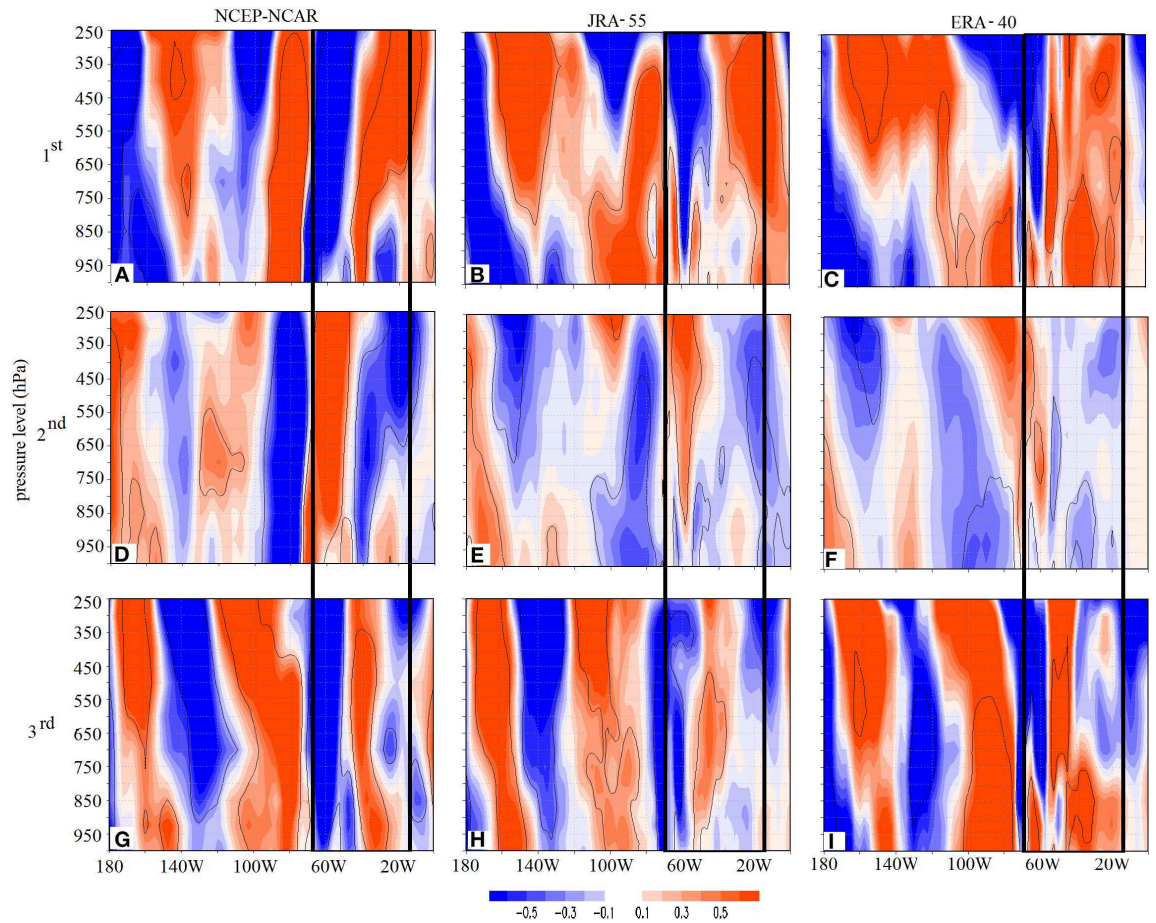

FIGURE 2 | Vertical profile of meridional wind component anomaly (m s^{-1}) averaged between 25°S and 22°S for the **(A)** 1st (1970–1976), **(B)** 2nd (1977–1996), and **(C)** 3rd (1997–2001) subperiods for NCEP-NCAR **(A,D,G)**, JRA-55 **(B,E,H)**, and ERA-40 **(C,F,I)** reanalysis. Statistically significant values for $\alpha = 0.05$ (*t*-Student) are surrounded by dotted isolines. The black rectangle includes the southeastern South America region.

convergent) climate conditions if the vertical profile is mostly barotropic, as shown by Coelho et al. (2015). The authors showed that, during the 2014 drought in the Brazilian southeast, there was a stationary anticyclonic anomaly with a barotropic vertical profile dominating the whole troposphere, which led to an anomalous dry period. Linear correlation analysis between the PDO index and the vertical distribution of geopotential height over southeastern Brazil (50–20°W) allowed the identification of the persistence of negative (positive) geopotential height anomalies during the positive (negative) PDO phase, from the surface to 700–300 hPa, depending on the dataset. The ERA-40 geopotential height data showed the shallowest barotropic pattern in the mentioned area in relation to JRA-55 and NCEP-NCAR datasets.

To investigate the homogeneity of the vertical pattern during distinct PDO phases, **Figure 2** shows the vertical profile of the meridional wind component anomaly for each subperiod and for the three data sources (NCEP-NCAR, JRA-55, and ERA-40 reanalysis) between 180°W and the Greenwich meridian for the latitudinal belt 25–22°S. This latitudinal belt was selected in order to identify the climatic influence of low-frequency wave propagation from the South Pacific Ocean to southeastern South America. In general, these three datasets showed similar vertical profile patterns of the meridional wind component. But, while the NCEP-NCAR dataset showed the most intense meridional wind anomalies (**Figures 2A,D,G**) and the most homogeneous pattern in the vertical dimension, with similar anomalies across the entire troposphere depth, particularly in the 70–20°W longitudinal belt, ERA-40 (**Figures 3B,E,H**) and JRA-55 (**Figures 3C,F,I**) v-wind anomalies were weaker and showed fewer homogeneous vertical patterns. JRA-55 and ERA-40 v-wind anomalies were also weaker in the 2nd subperiod in relation to the NCEP-NCAR data. Agreement of signal position in the three datasets occurs much more at high levels. At low levels, ERA-40 and JRA-55 v-wind anomalies presented the same signs as at high levels but in narrower columns, sometimes showing opposite signals in relation to NCEP-NCAR data, particularly in the 70–20°W longitudinal belt. Additionally, based on the three datasets, it seems that the stronger the wind signal was at high levels, the stronger it was at low levels. As mentioned by Coelho et al. (2015), barotropic conditions should exist to physically explain mean dry and wet periods over the southeast of Brazil. This

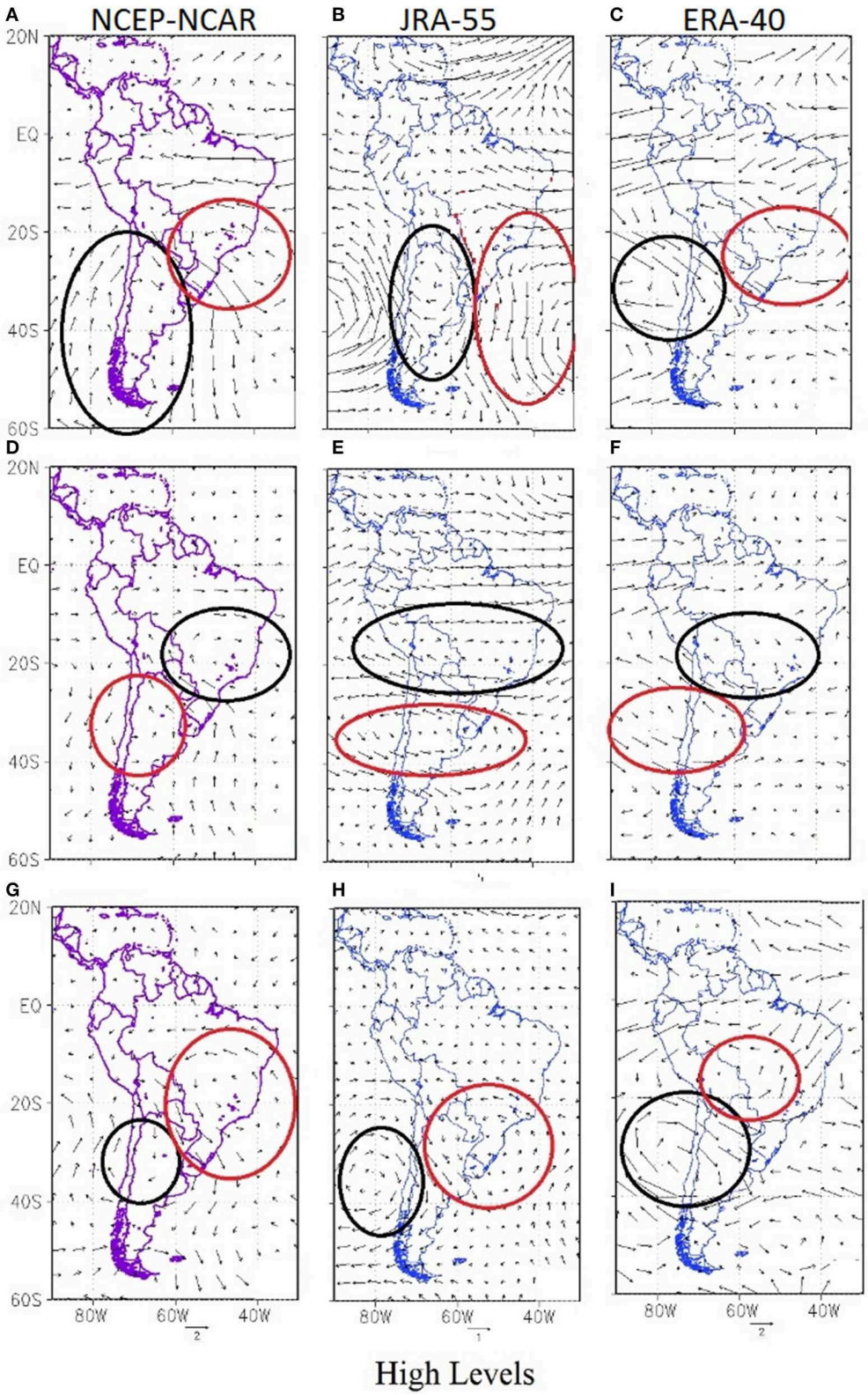

FIGURE 3 | High levels (500–200 hPa) mean wind vector anomaly (m s^{-1}) for the **(A–C)** 1st (1970–1976), **(D–F)** 2nd (1977–1996), and **(G–I)** 3rd (1997–2001) subperiods, for NCEP-NCAR **(A,D,G)**, JRA-55 **(B,E,H)**, and ERA-40 **(C,F,I)** reanalysis. Black (red) circles represent regions with a predominance of cyclonic (anticyclonic) wind movements.

statement is still valid during different PDO phases, as can be seen in the present study. Although showing the strongest signal and the best dataset to identify the dynamic differences between positive and negative PDO phases, the NCEP-NCAR reanalysis is not considered the best dataset to represent the South America precipitation, as indicated by Harada et al. (2016). In their study, the authors obtained the lowest linear correlation values for the NCEP-NCAR I precipitation and the highest values when they used JRA-55 data over the South American domain compared with GPCC data.

In the 1st and 3rd subperiods (**Figures 2A–C,G–I**, respectively), characterized by negative PDO phases, NCEP-NCAR v-wind (1st column) indicated southward and northward anomalies, respectively, to the west and east of 45°W throughout the whole troposphere, which is closely associated with mean low levels anticyclonic anomaly centered around 50°W; 18°S, as is clear from **Figure 3A**. The 2nd subperiod, characterized by the positive PDO phase, is marked by opposite v-wind anomalous signals in relation to the same longitude of 45°W (**Figures 2D–F**) and is associated with low levels cyclonic anomalies over the center of South America (**Figures 3D–F**). Roughly, vertical profiles of JRA-55 and ERA-40 v-wind anomalies showed similar patterns to the NCEP-NCAR data in upper levels and more distinct patterns at lower levels (**Figure 2**), still showing opposite signals in some places. In the three PDO phases, vertical homogeneity of JRA-55 v- wind anomalies at low levels was more similar to the NCEP-NCAR data, while ERA-40 was the most distinct. In general, negative signs to the west of 45°W (the intensified southward movement) in negative PDO phases (1st and 3rd lines; **Figures 2A–C,G–I**) were placed just to the west in the NCEP-NCAR data (**Figures 2A,G**) for all tropospheric levels. Otherwise, JRA-55 and ERA-40 v-wind anomalies did not present the same vertical distribution showing negative signs somewhat displaced to western positions, with the 300 and 700 level pattern distinct from that observed in the NCEP-NCAR data. In a broad sense, at the most western longitudes of **Figure 2**, considering not only south-eastern South America but also the whole longitudinal range (180°-Greenwich), vertical profiles of NCEP-NCAR v-wind anomalies (**Figures 2A,D,G**) also presented the most homogeneous patterns in vertical direction when compared with the JRA-55 (**Figures 2B,E,H**) and ERA-40 (**Figures 2C,F,I**) data. This aspect reveals a more barotropic behavior of the NCEP-NCAR data for the whole domain in relation to the other two datasets, corroborating the previous statement about linear correlation between PDO index and geopotential height.

Wind vector anomalies over South America obtained from JRA-55, ERA-40, and NCEP-NCAR reanalysis at different PDO phases can be seen in **Figures 3**, **4**, respectively, at integrated low (850–600 hPa) and high (500–200 hPa) levels. In general, all three datasets show anticyclonic and cyclonic anomalies over the central eastern South America region, during negative and positive PDO phases at low and high levels, respectively. This result is somewhat in agreement with the multidecadal oscillations suggestions made by Robertson and Mechoso (2000), Mo and Paegle (2001), and Zamboni et al. (2012) obtained from the NCEP-NCAR reanalysis I, although these authors did not make any association with the climatic patterns specifically influenced by ENSO or PDO as we did in this study.

Although a general agreement between the three reanalysis datasets is observed, there are differences in intensity and positioning of the anomalous circulation centers. For all three reanalyses, cyclonic and anticyclonic anomaly patterns at low (850–600 hPa, **Figure 3**) and high levels (500–200 hPa, **Figure 4**) showed different results. Compared with NCEP- NCAR and ERA-40, JRA-55 reanalysis presents the smallest wind anomaly values at low and high levels (**Figures 3**, **4B,E,H**)—scale wind vectors in the NCEP-NCAR and ERA-40 figures are twice the JRA-55—although with similar direction. In fact, considering the direction and intensity of wind anomalies for the three datasets, at low levels they are in closer agreement than at high levels (**Figures 3**, **4**). At high levels, the spatial pattern of the ERA-40 wind anomaly (**Figures 3C,F,I**) is more distinct from the NCEP-NCAR (**Figures 3A,D,G**) and the JRA-55 patterns (**Figures 3B,E,H**), as it is more difficult to identify cyclonic and anticyclonic anomalous circulations associated with PDO distinct phases. Black and red lines in **Figures 3**, **4** indicate cyclonic and anticyclonic anomalies, respectively.

Although ERA-40 high level horizontal wind anomaly in the 1st subperiod (**Figure 3C**) did not show a very similar pattern in relation to NCEP-NCAR and JRA-55 (**Figures 4A,B**), it was possible to see northeasterly anomalies over northeastern South American areas and northwesterly anomalies over central-south areas in the ERA-40 wind anomalies, both contributing to anticyclonic anomalous circulation at high levels. The cyclonic anomalous patterns observed in the 2nd subperiod for the three datasets presented lower values than those related to the 1st and 3rd subperiods, which is possibly explained by different time series length of the 2nd subperiod relative to the other two subperiods, as mentioned before. In the 2nd subperiod, a cyclonic anomalous circulation was observed at low levels in all three datasets, with the center close to the central-eastern area of the South America continent (**Figures 4D–F**). At high levels, the cyclonic anomalous circulation center was more displaced to interior areas for the JRA-55 and ERA-40 data (∼ 62°-58°W; 20°S) (**Figures 3E,F**) and to eastern areas for the NCEP-NCAR data (∼43°W; 20°S) (**Figure 3D**), covering in the latter a larger area. In the 3rd subperiod, the intensity and position of the anticyclonic anomalous circulation at low levels were in closer agreement in all three datasets (**Figures 4G–I**). However, at high levels, the NCEP-NCAR and JRA-55 anomalous circulation patterns (**Figures 3G,H**) differed from the ERA-40 (**Figure 3I**). In general, NCEP-NCAR and JRA-55 wind data showed at higher levels an anticyclonic anomalous circulation center near the southeastern coast of South America, while the ERA-40 data did not show a closed anticyclonic anomalous circulation. On the other hand, northwesterly and southeasterly anomalies in central-southern South America and central-northern Brazil (**Figure 3I**), respectively, indicated some agreement with the anticyclonic patterns shown by NCEP-NCAR and JRA-55 wind data at high levels.

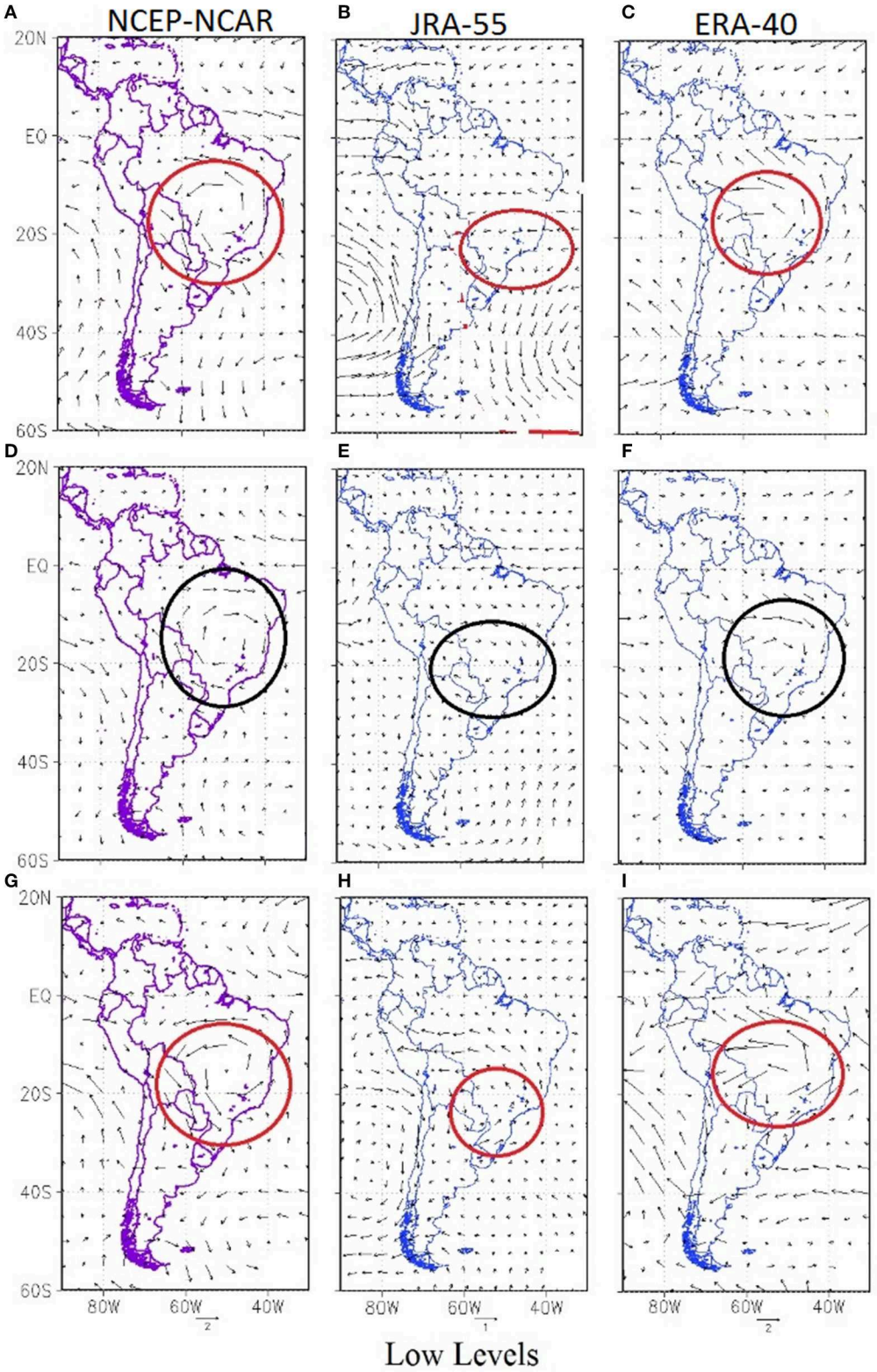

FIGURE 4 | Same as **Figure 3** but for low levels (850–600 hPa). Black (red) circles represent regions with a predominance of cyclonic (anticyclonic) wind movements.

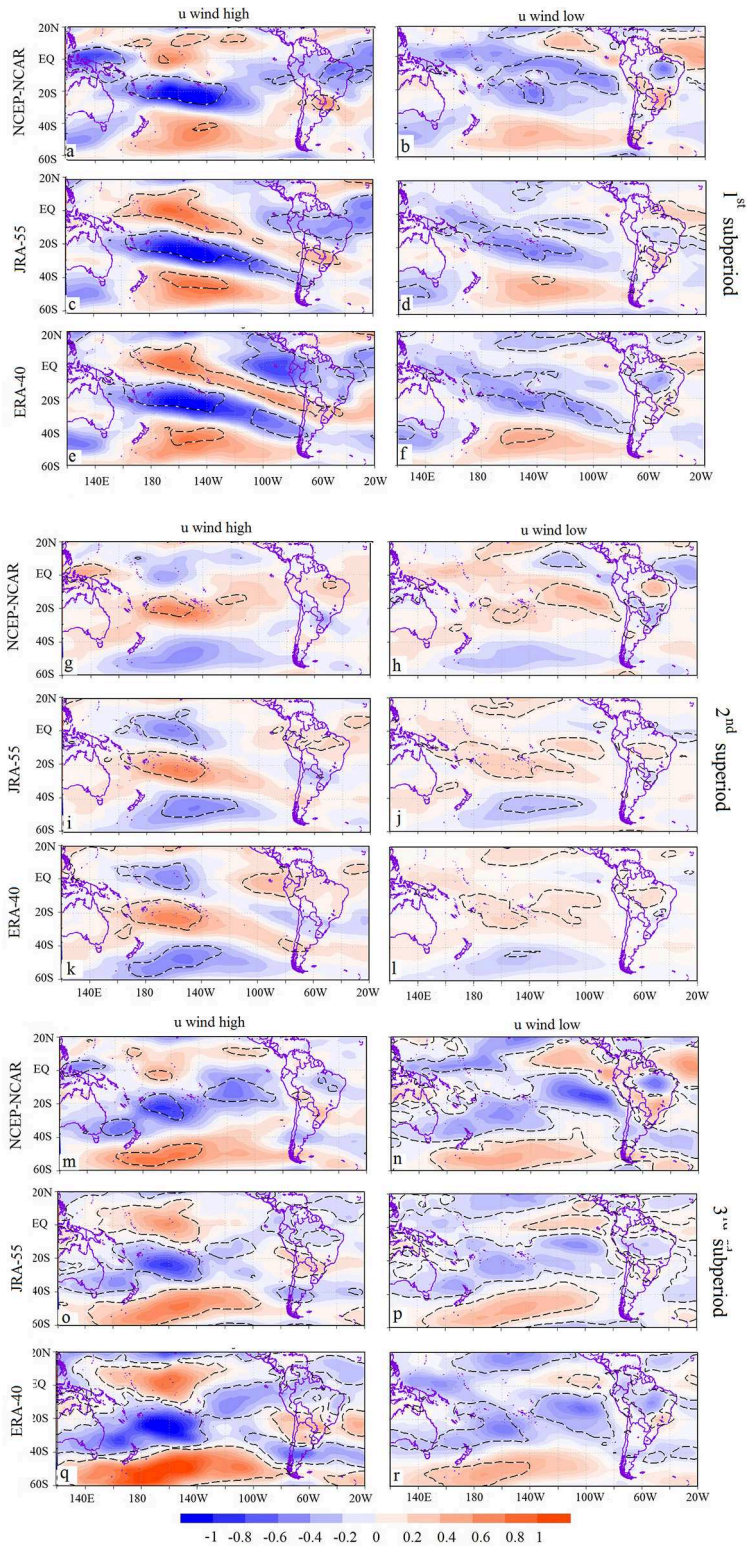

FIGURE 5 | Zonal wind anomaly at high levels (500–250 hPa) for **(a)** NCEP-NCAR, **(c)** JRA-55, and **(e)** ERA-40 reanalysis for the 1st subperiod. **(b,d,f)** The same as **(a,c,e)** but for low levels (850–600 hPa). **(g,i,k)** The same as **(a,c,e)** and **(h,j,l)** the same as **(b,d,f)** but for the 2nd subperiod. **(m,o,q)** The same as **(a,c,e)** and **(n,p,r)** the same as **(b,d,f)** but for the 3rd subperiod. JRA-55 u-wind anomaly values are multiplied by 2. Statistic significant values for $\alpha = 0.05$ (*t*-Student) are surrounded by dashed lines.

As the three datasets showed similarities but also certain differences in the anomalous circulation mean patterns, particularly at high levels (**Figure 3**), the analyses of the wind components were separated for each subperiod. **Figure 5** shows the u-wind anomalies and **Figure 8** the v-wind anomalies. Considering these three reanalysis datasets and the three subperiods, there were many similarities between the large-scale patterns of zonal wind anomalies, including the South Pacific and South American regions (**Figure 5**). The u- wind anomalies observed over equatorial Pacific areas during negative PDO phases were mainly negative, meaning an easterly wind was strengthening, while, in the positive PDO phase, these anomalies were positive, meaning an easterly wind was weakening. Strengthening and weakening easterlies were much stronger and spatially more spread at the high levels, with statistically significant values in larger areas. The most and least intense anomaly values occurred for the NCEP-NCAR and JRA-55 data, respectively, in particular for the 3rd subperiod. JRA-55 zonal wind data shows smaller values in all subperiods, at low and high levels, in comparison with NCEP-NCAR and ERA-40 data (**Figure 5**), according to what was observed in **Figures 3**, **4**.

Focusing on the South America region, all datasets presented negative and positive u-wind anomalies over northern/northeastern and central/central-eastern continental areas in the negative PDO phases (**Figure 5**), respectively. In the positive PDO phase (**Figures 5g–l**), an opposite pattern was observed, with positive and negative u-wind anomalies in northern/northeastern and central/central-eastern South American areas, respectively. Together with the v-wind anomalies (**Figure 6**), the u-wind patterns (**Figure 5**) lead to anticyclonic and cyclonic anomalous circulation centered all over central-eastern South America during negative and positive PDO phases, respectively, as was previously shown in **Figures 3**, **4**, for low and high levels.

In relation to the position of the strongest anomalies of the u-wind component over South America, there was more agreement between NCEP-NCAR and ERA-40 patterns. Considering the three subperiods, JRA-55 u-wind anomalies at low levels (**Figure 5**) seemed to show a westward displacement of the strongest negative and positive signals in northern South America, respectively, for negative and positive PDO phases, in relation to the NCEP-NCAR and the ERA-40 datasets, and this was marked by a black rectangle in the figure. Additionally, the opposite and significant signs of the low-level u-wind anomalous patterns over the equatorial eastern Pacific (140–90°W), placed westward to the strongest anomaly observed in the NCEP-NCAR and ERA-40 datasets over South America, during reversal PDO phases, were not observed in the JRA-55 data. In fact, the JRA-55 u-wind data showed the intensification of the trade winds during negative PDO phases (**Figures 5d,p**) and its weakness during positive the PDO phase (**Figure 5j**), in contrast with the NCEP-NCAR and ERA-40 signal. This low-level u-wind aspect was observed both for the positive and negative PDO phases, showing opposite patterns in each PDO phase, and this is an important difference between the three databases. At high levels, JRA-55 u-wind data at eastern equatorial Pacific areas were in closer agreement with the other two reanalyses, presenting the same signal for each PDO phase.

Another important distinction between the three reanalysis datasets can be observed in high-level zonal wind anomaly fields over the Pacific Ocean basin, from 20°N to 60°S, as shown in **Figure 5**. Both NCEP-NCAR and ERA-40 showed more agreement between them, while the JRA-55 fields presented the most distinct patterns of changing signals in the meridional direction. While NCEP-NCAR and ERA-40 datasets show, from north to south, positive, negative, and positive anomalies for negative PDO phases (1st and 3rd subperiods), **Figure 5**, JRA-55 data presented a somewhat opposite pattern, with the northern latitudes featuring negative anomalies and subtropical latitudes positive ones.

Although these differences over the Pacific Ocean were observed, all three reanalyses showed more similar patterns of high level u-wind means over continental areas of South America, with negative and positive anomalies at north and subtropical latitudes during the PDO negative phases and the opposite pattern during the positive phase. On the other hand, at low tropospheric levels, JRA-55 showed the most distinct zonal wind anomaly pattern over South America when compared with NCEP-NCAR and ERA-40, the most intense negative anomaly in northern areas were displaced westward. In the positive PDO phase (2nd subperiod) (**Figures 5g–l**), the wind zonal anomalies at high levels showed the opposite patterns for the three reanalysis datasets, even considering those differences observed for JRA-55. Over equatorial latitudes, while NCEP-NCAR and ERA-40 high levels zonal wind changed the anomaly signals between the western and eastern Pacific in opposite PDO phases, JRA-55 presents a homogeneous anomaly pattern in the zonal direction, from 140°E to 20°W, contrasting with the other two datasets. This characteristic may cause differences in low frequency wave propagation through the Pacific Ocean. As a consequence of these features in positive (negative) PDO phases, NCEP-NCAR and ERA-40 high-level zonal wind anomalies showed divergent (convergent) anomalous patterns close to 140°W at equatorial latitudes, possibly favoring (reducing) convection in this area. The contrasting convergent and divergent anomalous patterns in distinct PDO phases may be associated with the Walker cell zonal displacement during distinct climatic forcing, which must be better addressed in physical approaches. Moreover, the reasons for the different representation seen in the JRA-55 zonal wind anomalies should be better understood.

Analysis of the v-wind component anomalies over South Pacific and South America (from 120°W to 120°E), shown in **Figure 6**, allows us to better understand the similarities and differences between the three datasets in the three subperiods (1970–1976; 1977– 1996, and 1997–2001). Focusing on the NCEP-NCAR v-wind anomaly, the values showed anomalous signals over South America contributing to anticyclonic and cyclonic anomalous circulation during the negative and positive PDO phases, respectively. During the negative PDO phases (**Figure 6**), the strongest negative v-wind anomalies were observed over central-southeastern South America and positive signs over central- eastern areas, defining an anticyclonic anomalous circulation. During the positive PDO

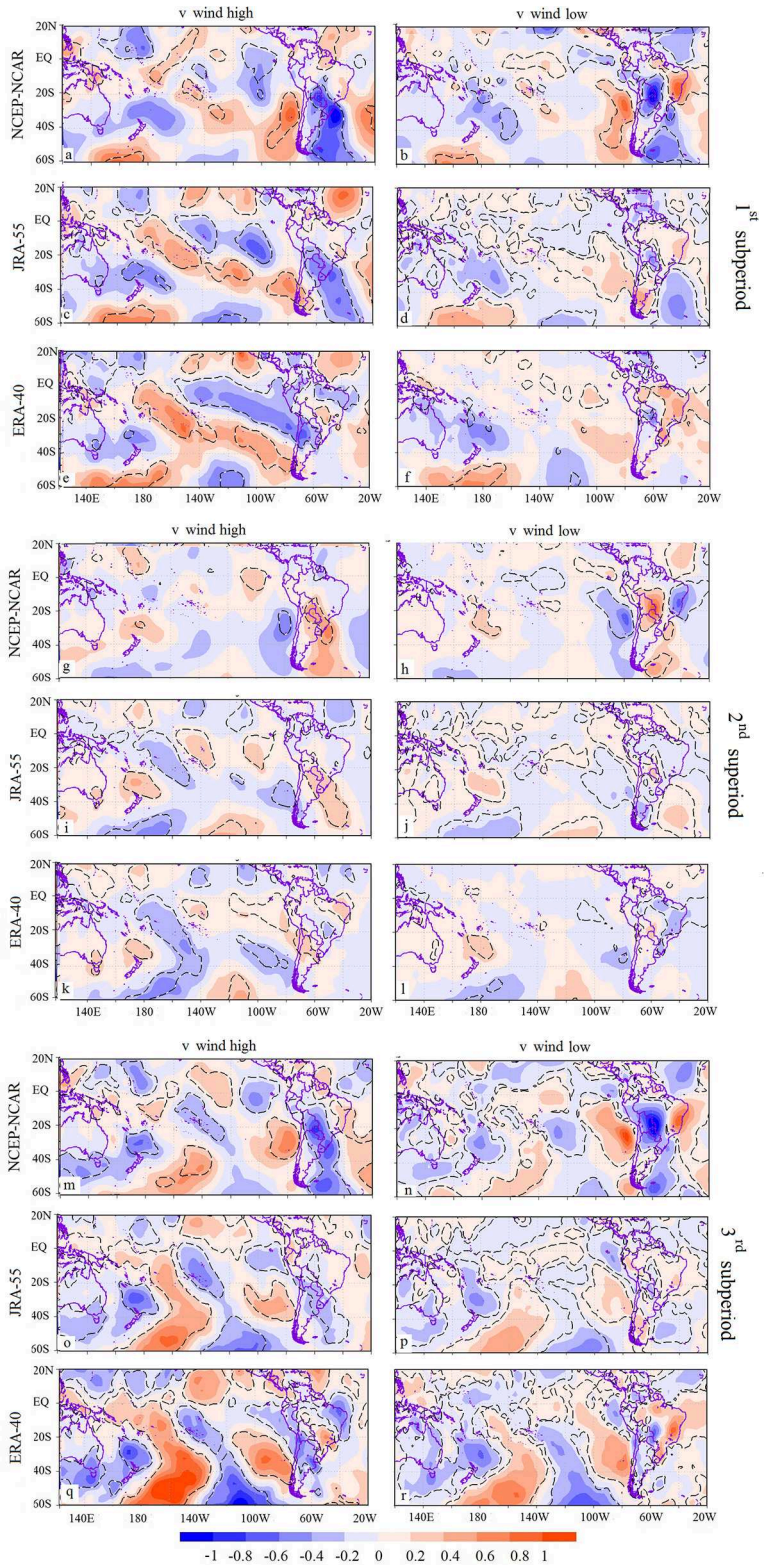

FIGURE 6 | Same as **Figure 5** but for meridional wind anomaly.

phase (**Figures 6g–l**), an opposite pattern of v-wind anomaly was observed over South America. Besides this, significantly positive (negative) anomalous values were observed over the southeastern Pacific, along the South America western coast, during negative (positive) PDO phases. This pattern over the South America western coast seemed to be displaced westward and southward for the ERA-40 and JRA-55 v-wind anomalies in all three subperiods, and this was mainly observed at high levels. At low levels, although JRA-55 and ERA-40 wind anomalies were weaker than the NCEP-NCAR values, positions of the strongest signal along the western coast of South America in the three databases were in greater agreement than that those at high levels. Another important difference between the three datasets refers to the orientation of the main v-anomaly values: while NCEP-NCAR and JRA-55 showed areas with the strongest v-wind anomalies, preferably oriented in the north-south direction, ERA-40 data showed areas with the strongest v- wind anomalies covering more zonal directions. This is probably related to the representation of the wave propagation disturbances in these regions. Although the ERA-40 v-wind showed the strongest anomalies in a more zonal direction (which is observed for the first two subperiods), it showed an anomalous patterns similar to the NCEP-NCAR data over South America but with a small southward displacement. In the case of JRA-55, the westward wave pattern displacement was stronger than in the case of ERA-40 when comparing both with NCEP-NCAR data. This aspect was stronger in the 1st subperiod but was also noted in the 3rd subperiod, both negative PDO phases. In the positive PDO phase, weakening of the South Pacific anticyclone eastern branch in the JRA-55 v-wind data also displaced westward in relation to NCEP-NCAR and ERA-40 data, i.e., JRA-55 v-wind anomalies close to the South America western coast were in many cases displaced to western areas.

Additionally, with continental areas, we analyzed the wind climatic patterns over the Pacific Ocean where the PDO takes place. In equatorial Pacific areas, meridional wind anomalies

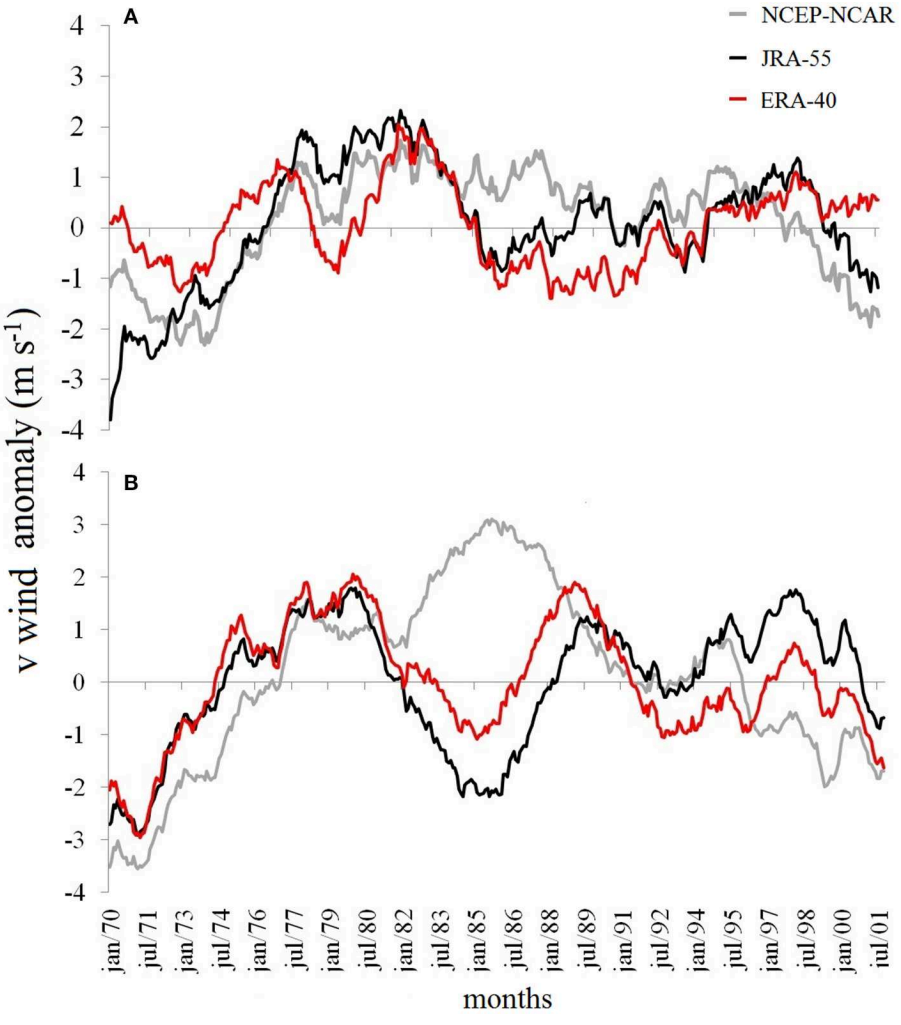

FIGURE 7 | Monthly meridional wind component averaged over (62°W, 25°S; 58°W, 18°S), where LLJ commonly assumes higher values (over Bolivia and Paraguay), at **(A)** 250 hPa and **(B)** 850 hPa, in the 1970–2001 period, for NCEP-NCAR (gray), JRA-55 (black) and ERA-40 (red) datasets.

(both for low and high levels) from the three reanalysis datasets were analyzed and featured opposite patterns in PDO reversal phases, similar to the zonal wind anomalies. During the negative PDO phases (**Figures 6a–f,m–r**), we observed positive and negative mean v-wind anomalies longitudinally placed along the Pacific equatorial belt in western and eastern areas, respectively, delimited by the coordinates 120–80°W and 160–120°W, in the case of the NCEP-NCAR data (**Figures 6a,b,m,n**). This dipole pattern over the equatorial Pacific was well marked in the NCEP-NCAR v-wind anomalies, while the JRA-55 and ERA-40 data showed more unclear patterns. In these three datasets, the dipole pattern over the equatorial Pacific was usually stronger at high levels. Although the strongest positive and negative anomalies of JRA-55 v-wind over the Pacific Ocean seemed to be shifted in relation to the NCEP-NCAR data (see the Pacific South American western coast and continental areas, **Figures 6m–o**), the global impact over the continent was not so distinct, as shown in **Figure 4**. Another significant aspect observed in opposite PDO phases was the v-wind anomaly dipole pattern observed over higher latitudes, from the Australian east coast toward eastern oceanic areas, from 170°E to 120°W and from 20 to 50°S, with the strongest signal at high levels. During the negative (positive) PDO phase, the v-wind anomaly over this area is negative (positive) close to the Australian eastern coast and positive (negative) over eastern adjacent oceanic areas. All three datasets showed this zonal dipole over western subtropical Pacific areas (**Figure 6**), with JRA-55 data showing the weakest signal. This dipole pattern to the east of Australia, in reverse PDO phases, may be associated with low-frequency wave propagation, characterizing the PDO variability scale since it was observed in the three datasets.

The meridional wind over the central South American area coincided with the low-level jet (LLJ) locations in the continent, having the strongest values over Bolivia and Paraguay (Marengo et al., 2004). The LLJ northerly flow takes moisture and heat from northern to southern areas in the continental scale, adding energy to convective systems in southern areas, mainly during the summer season when continental heating makes the trade winds move toward the continental thermal low. Values of meridional wind anomalies at 850 hPa from NCEP-NCAR, ERA-40, and JRA-55 reanalysis expressed a mean decadal oscillation throughout the entire analyzed period, with negative anomalies (stronger northerly flow) in negative PDO phases and positive anomalies (weaker northerly flow) in the positive PDO phase (**Figure 7**). Although we observed similarities, ERA-40 and JRA-55 presented some distinct aspects from the NCEP-NCAR meridional anomalies, especially over the 1982–1989 period at low level (850 hPa) (**Figure 7b**) and the 1983–1994 period at high level (250 hPa) (**Figure 7a**). While the meridional data from the NCEP-NCAR reanalysis always presented positive anomalies over the LLJ area during the positive PDO phase, showing a weakening of the northerly meridional flow, ERA-40 and JRA-55 meridional components indicated a more variable pattern in time, with both weakening and strengthening of the meridional flow during the PDO positive phase. The differences in the meridional component anomaly over the LLJ area were smaller between ERA-40 and JRA-55 when compared with the NCEP-NCAR component, which can be partially associated with higher spatial resolutions in the first two reanalyses (1.25 and 1.0 degrees in ERA-40 and JRA-55, respectively) in relation the NCEP-NCAR resolution (2.5 degrees). In summary, it is possible to conclude that distinct v-wind signals between the three datasets showed important variability, deserving some attention once the meridional flow over South America had an important impact on precipitation systems developed at higher latitudes. New approaches in the JRA-55 data assimilation system (Harada et al., 2016) could possibly explain part of the differences detected, which may be better explored in further studies.

Precipitation Analysis

The circulation analysis based on the NCEP-NCAR, JRA-55, and ERA-40 reanalysis datasets showed the association between reversal PDO phases and opposite circulation anomalies over South America. Negative PDO phases observed in the 1970–2001 period were significantly characterized by strengthening of easterly flow at low and high levels over northeastern areas of South America and also by the strengthening of the northerly flow over central continental areas, which were particularly important at low tropospheric levels once the moisture and warm air transported from the north to the south impacted the climate in these regions. Precipitation fields obtained from the three reanalysis datasets compared with the GPCC data in opposite PDO phases were used here to indicate the differences observed in the moisture advection.

Based on the GPCC dataset, precipitation anomalies (**Figures 8a,e,i**) in the PDO phases can be associated with a dipole-like pattern over the eastern South America region, covering an area delimited by the rectangle, Area 1 (showing the Brazilian states of Minas Gerais, Bahia, Goiás, Tocantins, Rio de Janeiro, and Espírito Santo), and the circled area, Area 2 (covering the Brazilian states of São Paulo, Paraná, Santa Catarina, Rio Grande do Sul, Mato Grosso do Sul, eastern Paraguay, and part of Bolivia). The negative PDO phases (1st and 3rd subperiods) (**Figures 8a,i**) were associated with less precipitation in Area 1, the central-eastern area, and more precipitation in Area 2, the southeastern region. The positive PDO phase (2nd subperiod) (**Figure 8e**) was associated with the opposite pattern in Area 1 and Area 2 for the GPCC data, with more precipitation in Area 1 and less precipitation in Area 2, in relation to the respective climatological means. These two areas in central-eastern South America, showing strong precipitation anomalies, were selected in order to identify the climatic influence of low frequency wave propagation from South Pacific Ocean to South America, associated with the fact of presenting opposite signals. Actually, the precipitation anomalies observed over Area 1 were much more spread over South American continental areas than those delimited by the rectangle area in negative and positive PDO phases (**Figures 8a,e,i**), reaching central and southern continental areas and covering central regions of Brazil (Mato Grosso state and south of Pará state), Bolivia, and areas of northern Argentina. This enlarged area over South America also showed a dipole-like behavior associated with the opposite PDO phases, which is seen in **Figure 8**. Bolivia

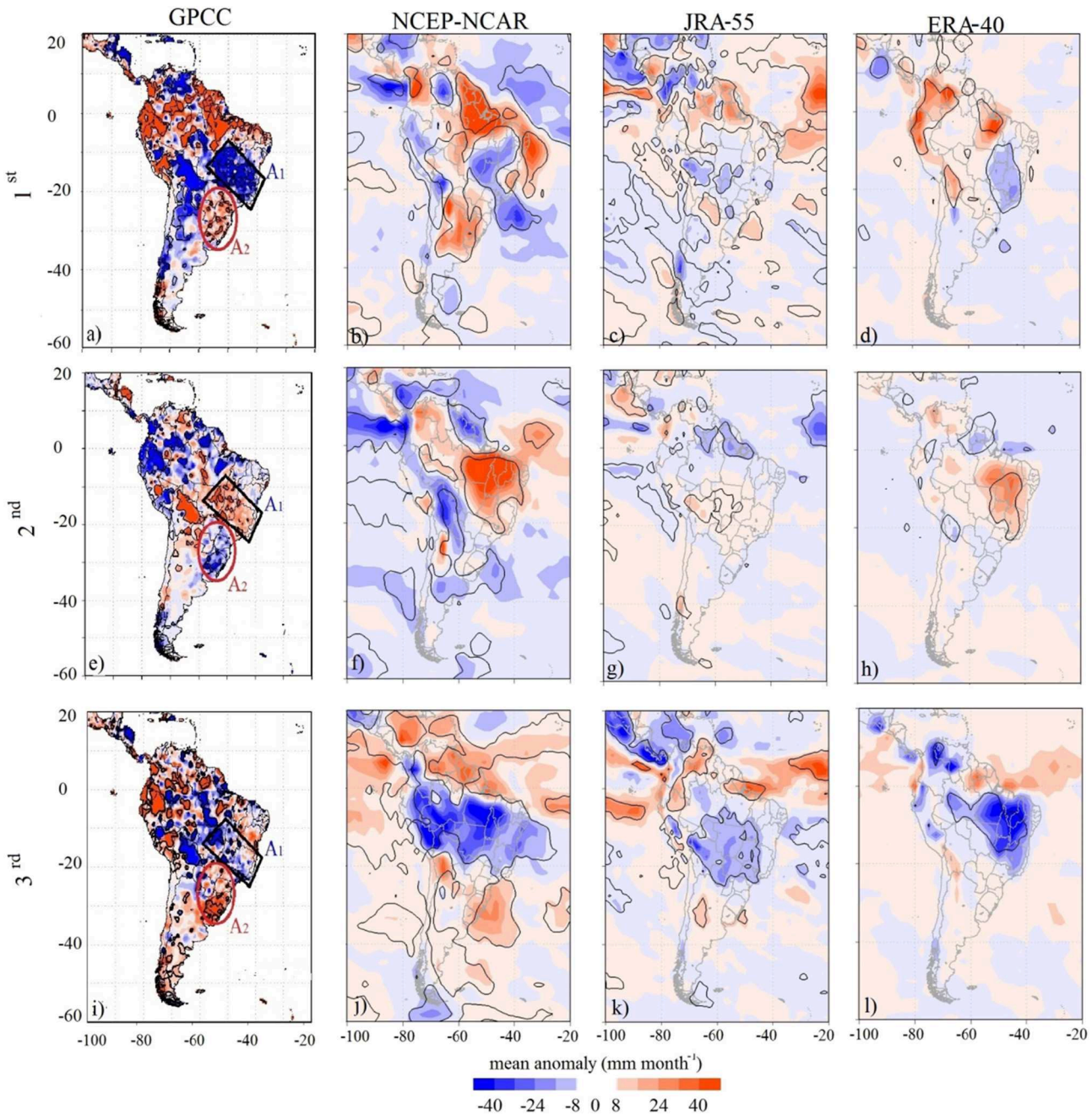

FIGURE 8 | Precipitation mean anomalies in the **(a–d)** 1st, **(e–h)** 2nd, and **(i–l)** 3rd subperiods from 1970 to 2001, for the GPCC, NCEP-NCAR, JRA-55, and ERA-40 datasets. Area A1 (rectangle), delimited by 295° W-315° W; 22° S-15° S and Area A2 (circle), delimited by 300° W-310° W; 32° S-25° S).

in particular, located in the center-west of South America, is marked by strong precipitation anomalies both during positive and negative PDO phases, making it a potential area strongly associated with the PDO variability.

In a general sense, we can say that all the three reanalysis datasets showed spatial patterns of precipitation anomalies over the dipole area (southeast-central South America) with the same signal between them during the considered PDO phases, but with different intensities. Reanalysis anomalies also had the same signal as in the GPCC anomalies (**Figure 8**). Similar to the circulation patterns seen in the previous figures, the NCEP-NCAR precipitation anomalies were also the strongest when compared with the JRA-55 and ERA-40 anomalies. Temporal evolution of the mean precipitation anomaly over Area 1 and Area 2 from 1970 to 2001 during the three PDO phases showed a clear decadal variability in both areas (**Figures 9a,b**), particularly

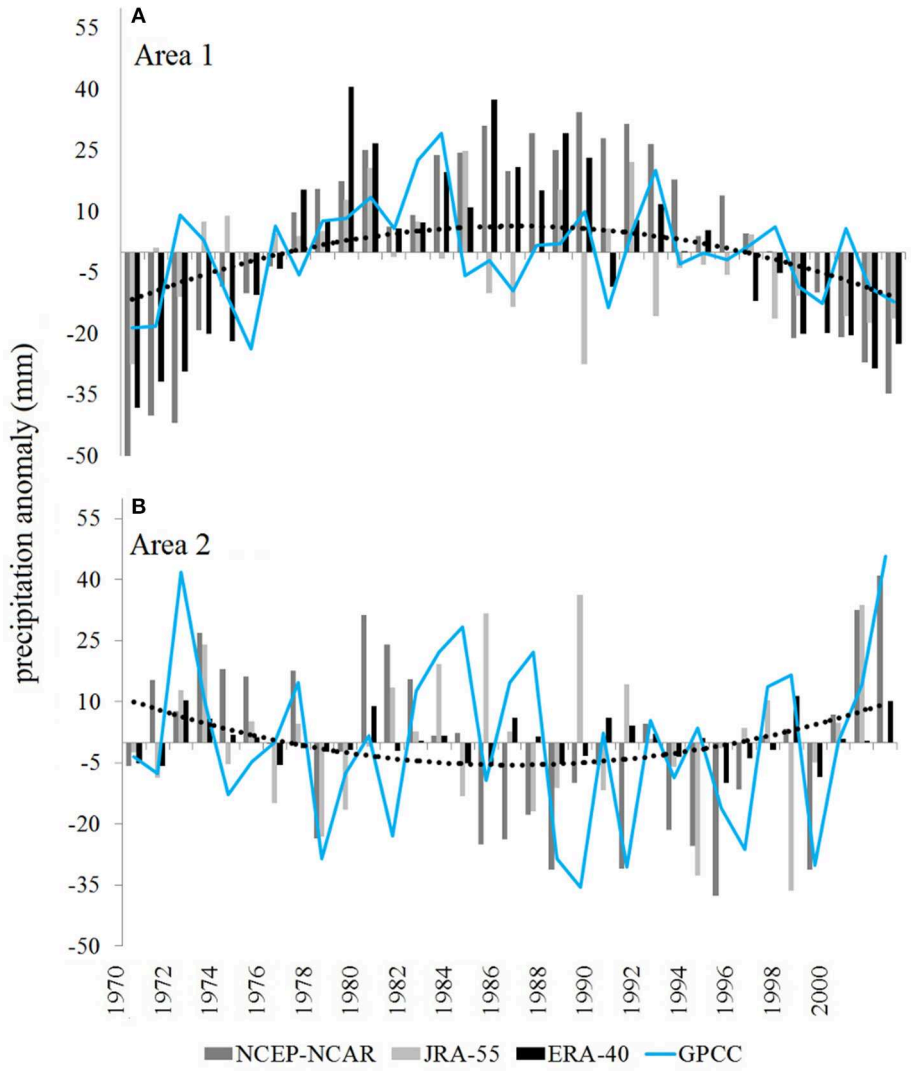

FIGURE 9 | Temporal evolution of precipitation anomaly from GPCC (blue line) dataset, NCEP-NCAR reanalysis I (gray bar), JRA-55 (light gray bar), and ERA-40 (black bar) reanalysis data for the 1970–2001 period, for areas **(a)** A1 and **(b)** A2 as in **Figure 8**. Polynomial of degree two for the GPCC data is represented by dotted lines.

for the GPCC and the NCEP- NCAR data. The precipitation over Area 1 showed a much stronger decadal variability than over Area 2 for the GPCC and the reanalysis data. Also, the precipitation time series in Area 1 for the three reanalysis datasets were more similar to each other than those for Area 2. The GPCC data, in comparison to the reanalysis, presented larger mean values in the southeastern South America region, particularly in the Area 2. Over the central-eastern South American region (Area 1), NCEP-NCAR precipitation was, on average, 57% larger than GPCC values and 35% and 46% larger than JRA-55 and ERA-40 values, respectively.

Although some distinctions could be observed among the four considered datasets, mostly related to intensity, we can suggest that the decadal low frequency precipitation patterns obtained from the reanalysis datasets, NCEP-NCAR, JRA-55, and ERA-40, particularly over eastern areas of South America, have the same signal as those presented by the GPCC precipitation in almost all cases characterizing the dipole pattern over this area.

Maps of linear correlation coefficient values between monthly GPCC and those from the reanalysis over the tropical South America domain (25°S−10°N) showed the highest and the most frequent higher values for JRA-55 data, while NCEP-NCAR and ERA-40 data showed smaller correlation values, as seen in **Figure 10**. This result allows us to suggest that, although JRA-55 was the reanalysis dataset showing the weakest anomalous signals related to the PDO phases (seen in **Figures 8**, **9**), both for precipitation and atmospheric circulation, it seems to be the best candidate to more reliably represent the regional climate.

DISCUSSIONS AND CONCLUSIONS

In this paper, the circulation and precipitation climate patterns over the South American domain obtained from NCEP-NCAR (reanalysis I), JRA-55, and ERA-40 reanalysis datasets were intercompared during the period 1970–2001 in order to verify their climatic association with the Pacific Decadal Oscillation. The entire period included three distinct PDO phases, 1970–1976 (negative phase), 1977–1996 (positive phase), and 1997–2001 (negative phase). The use of more recent reanalysis datasets, such as JRA-55 and ERA-40, allowed us to evaluate possible data dependence of the previous findings by Robertson and Mechoso (2000), Mo and Paegle (2001), Zamboni et al. (2012), and Silva et al. (2016), which considered only the NCEP-NCAR reanalysis I dataset over the South America region.

The intercomparison between NCEP-NCAR, JRA-55, and ERA-40 reanalysis data developed in the present study suggested that, in general, all three datasets showed similar climatic signals during the three PDO subperiods but with distinct intensities for circulation and precipitation variables, responding to the question made at the beginning. The observed patterns of anomalies for different PDO phases appeared in all reanalysis datasets, leading us to conclude that the physical meaning from PDO influence was independent of the datasets. NCEP-NCAR reanalysis I, in comparison with JRA-55 and ERA-40, always indicated the strongest signal, both for circulation and precipitation. The low frequency of high-level geopotential height showed opposite patterns during positive and negative PDO phases from the South Pacific to South America. During the negative (positive) PDO phases, central-eastern South America was characterized by positive (negative) geopotential height anomalies extending from the low to the middle or upper troposphere depending on the dataset. Thus, we can say that the mean low frequency flow propagation over the South Pacific during negative and positive PDO phases reached central-eastern South America with opposite signals, contributing to the modulation of the local climate. The reasons for differences brought by the three reanalysis datasets should be investigated in further studies, which might attempt to indicate what the related causes are.

Associated with reversal geopotential height anomalies in each PDO phase over eastern South America, the northerly flow over the central continental area, where the LLJ commonly takes place, was characterized by opposite anomaly signals. During negative PDO phases, the northerly flow intensified, while it weakened during the positive phase. The strengthening and weakness of the meridional wind at the center of South America during negative and positive PDO phases were associated with anticyclonic and cyclonic anomalous circulation over this area, respectively. Although the low-level jet was mainly characterized at low atmospheric levels (∼850 hPa), meridional wind anomalies of the same signal were observed from low to upper levels during reversal PDO phases. That is, the vertical dimension of South American circulation was entirely modified in each PDO phase, which was observed in the three datasets. NCEP-NCAR reanalysis I showed meridional wind at the LLJ area to be about 5 and 12% greater than the JRA-55 and the ERA-40 values, respectively, though in all the three datasets the same anomalous pattern was observed. Results of the circulation and precipitation patterns over the entire South American domain during distinct PDO phases were not mentioned in previous studies except by Silva et al. (2016). The results obtained in Silva et al. (2016), with the NCEP-NCAR reanalysis I, and those obtained with JRA-55 and ERA-40 in this study, although showing similar signals, presented differences in intensity, and the results observed here were much clearer. Physically, the northerly flow strengthening and weakening in negative and positive PDO phases, respectively, constituted the most important finding, and this was not mentioned in previous studies. Both Villamayor et al. (2018) and Andreoli and Kayano (2004), studying the PDO influence on the northern South America climate, for distinct periods of time, reached the conclusion of precipitation suppression.

Anticyclonic and cyclonic anomalies observed at low and high levels of reversal PDO phases can be associated with drier and wetter periods, respectively, once a barotropic troposphere is assumed. Vertical profiles for geopotential height and wind data almost showed barotropic behavior over southeastern South America, which can be associated with drier and wetter observed patterns, as suggested by Coelho et al. (2015) who explained the occurrence of an extreme drought in the southeast of South America during the summer of 2014. When compared to the NCEP-NCAR and JRA-55, ERA-40 data showed the shallowest barotropic vertical troposphere over the southeastern South America latitudinal belt (22–25°S) during the three PDO phases, while the NCEP- NCAR data showed the deepest one.

Over equatorial latitudes of the Pacific Ocean, the intercomparison of datasets allows us to identify important differences. For positive and negative PDO phases, NCEP-NCAR and ERA-40 high-level zonal wind anomalies showed divergent and convergent patterns close to 140°W at equatorial latitudes, respectively, favoring and suppressing convection processes at low levels, respectively. This feature was not observed in the JRA-55 wind data, indicating distinct representations of the positioning of Walker cells by the three reanalysis datasets. Additionally, opposite and significant signals of the zonal wind anomalies at low tropospheric levels in NCEP-NCAR and ERA-40 datasets, during reversal PDO phases, located over the equatorial eastern Pacific in the western South America coast, were not observed in the JRA-55 data.

The analysis of precipitation patterns during opposite PDO phases, based on monthly GPCC datasets, NCEP-NCAR, JRA-55, and ERA-40 reanalysis, showed, in general, the dipole pattern over eastern of South America, with changing signals between the central-eastern and southeastern areas. The central-eastern South America area (Area 1) presented negative (positive) precipitation anomalies during the negative (positive) PDO phases, while the southeastern area (Area 2) presented the opposite pattern. NCEP-NCAR reanalysis I showed the most intense precipitation anomalies

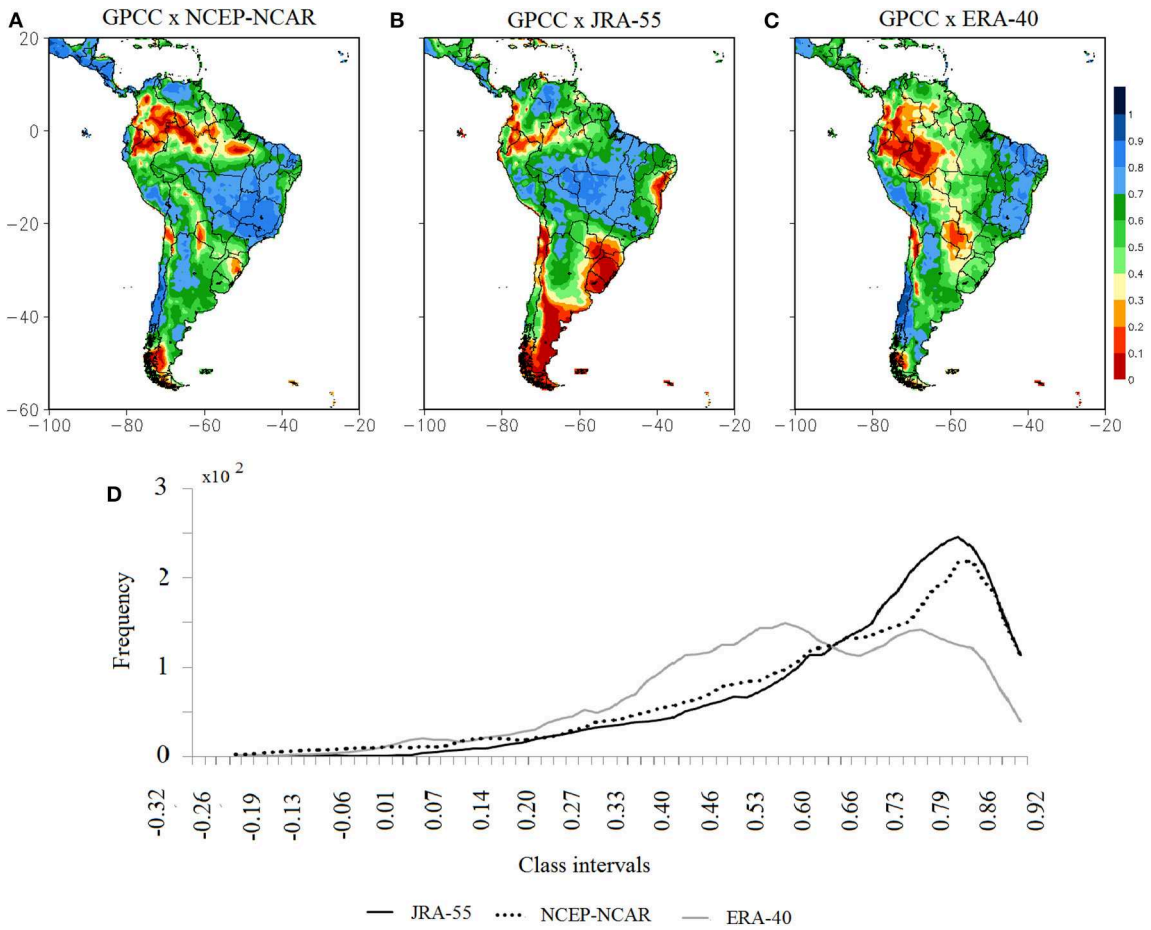

FIGURE 10 | Linear correlation coefficient between monthly GPCC and **(A)** NCEP-NCAR reanalysis I, **(B)** JRA-55, and **(C)** ERA-40, from 1970 to 2001, for the tropical South America area (25° S−10° N). **(D)** Linear correlation coefficient frequency distribution for each map in **(A–C)**. The data used in the correlation computation presents original seasonality.

over the eastern South American dipole during the three analyzed PDO phases, and this can be associated with the strongest circulation patterns in relation to JRA-55 and ERA-40 datasets.

Differences observed in these three datasets can be partially caused by discrepancies in the assimilation processes in the numerical models before and after 1978, when satellite data had just begun to be incorporated. Bromwich and Fogt (2004) showed important distinctions between NCEP-NCAR and ERA-40 500 hPa geopotential height over South Pacific high latitudes (60–70°S; 130–150°W) previously to 1978. They also discussed the increase in the skill of the NCEP-NCAR and ERA-40 reanalysis, compared with *in situ* observations, over Southern Hemisphere high latitudes and the Antarctica region for data observed before and after 1978. Other studies carried out for different global regions found distinct results in relation to different reanalysis datasets. For example, Cook and Vizy (2016) did not find any important differences between ERA- 20C, ERA-40, JRA-55, and NCEP-NCAR reanalysis datasets when they analyzed the maintenance of the African occidental monsoon system associated with the Walker circulation variability through evaporation and SST data.

Although NCEP-NCAR reanalysis I showed the strongest anomalous signals, making the detection of low frequency signal easier, the oldest reanalysis dataset was taken into account here. JRA-55, being the newest reanalysis dataset, shows the weakest PDO influence signal among the three datasets. Linear correlation coefficients between GPCC and the precipitation from reanalysis data indicated that JRA-55 is the best candidate to reliably represent the climate over tropical South America since the highest values were obtained with this dataset, a result corroborated by Harada et al. (2016). Part of the skill of JRA-55 in calculating precipitation probably comes from the four-dimensional variational analysis (4D-Var) (DAS 3rd generation) used in the data assimilation system (Harada et al., 2016). Also, ERA-40 reanalysis was obtained by applying the older 3D-Var technique (DAS 2nd generation) to the data assimilation system, which may have led to lower skill. In order to provide more detailed categorization of climate patterns related to PDO

influence over South America, seasonal analysis can be carried on in further studies.

DATA AVAILABILITY STATEMENT

Publicly available datasets were analyzed in this study. This data can be found here: https://www.esrl.noaa.gov/psd/data/gridded/data.ncep.reanalysis.html.

AUTHOR CONTRIBUTIONS

MS: initiated the study, analyzed the results, and was responsible for the final editing. CS: carried out the data processing, prepared the work results, participated in the introduction, final editing and analyzed the results. TA: analyzed and verified the results, contributed to the debate, gave suggestions and ensured the scientific validity of the work. AD and NP: analyzed the results, contributed to the debate, gave suggestions, and verified the results.

ACKNOWLEDGMENTS

The authors acknowledge CNPq (N. 304298/2004-0) and FAPESP (N. 2017/09308-9) for the financial support. TA was partially supported by the Brazilian National Institute of Science and Technology (INCT) for Climate Change funded by CNPq Grant Number 573797/2008-0 and FAPESP Grant Numbers 2008/57719-9 and 2017/09659-6. The first and second authors acknowledge the postgraduate program in Physical Geography of the University of São Paulo, Brazil, which provided the technical support for the research and development. The authors acknowledge the suggestions made by the reviewers.

REFERENCES

Adler, R. F., Huffman, G. J., Chang, A., Ferraro, R., Xie, P., Janowiak, J., et al. (2003). The version-2 global precipitation climatology project (GPCP) monthly precipitation analysis (1979-present). *J. Hydrometeor.* 4, 1147–1167, doi: 10.1175/1525-7541(2003)004<1147:TVGPCP>2.0.CO;2

Andreoli, R. V., and Kayano, M. T. (2004). Multi-scale variability of the sea surface temperature in the Tropical Atlantic. *J. Geophys. Res. Oceans* 109:C2. doi: 10.1029/2003JC002220

Bjerknes, J. (1969). Atmospheric teleconnections from the equatorial Pacific. *Mon. Wea. Rev*, 97, 163–172. doi: 10.1175/1520-0493(1969)097<0163:ATFTEP>2.3.CO;2

Bromwich, D. H., and Fogt, R. L. (2004), Strong trends in the skill of the ERA-40 and NCEP- NCAR reanalyses in the high and middle latitudes of the Southern Hemisphere, 1958–2001. *J. Clim.* 17, 4603–4619. doi: 10.1175/3241.1

Coelho, C. A., de Oliveira, C. P., Ambrizzi, T., Reboita, M. S., Carpenedo, C. B., Campos, J. L., et al. (2015). The 2014 southeast Brazil austral summer drought: regional scale mechanisms and teleconnections. *Clim. Dyn.* 46, 3737–3752. doi: 10.1007/s00382-015-2800-1

Cook, K. H., and Vizy, E. K. (2016). The Congo Basin Walker circulation: dynamics and connections to precipitation. *Clim. Dyn.* 47, 697–717. doi: 10.1007/s00382-015-2864-y

Dee, D. P., Uppala, S. M., Simmons, A. J., Berrisford, P., Poli, P., Kobayashi, S., et al. (2011). The ERA-Interim reanalysis: configuration and performance of the data assimilation system. *Q. J. R. Meteorol. Soc.* 137, 553–597. doi: 10.1002/qj.828

Ding, Q., Steig, E. J., Battisti, D. S., and Küttel, M. (2011). Winter warming in West Antarctica caused by central tropical Pacific warming. *Nat. Geosci.* 4, 398–403. doi: 10.1038/ngeo1129

Duchon, C. E. (1979). Lanczos filtering in one and two dimensions. *J. Appl. Meteorol.* 18, 1016–1022.

Gershunov, A., and Barnett, T. P. (1998). Interdecadal modulation of ENSO teleconnections. *Bull. Am. Meteorol. Soc.* 79:2715.

Grimm, A. M., and Ambrizzi, T. (2009). "Teleconnections into South America from the tropics and extratropics on interannual and intraseasonal timescales," in *Past climate variability in South America and Surrounding Regions: from the last glacial maximum to the Holocene, Developments in Paleoenvironmental Research*, eds Vimeux, F., Sylvestre, F., and Khodri, M. (Springer), 159–191.

Harada, Y., Kamahori, H., Kobayashi, C., Endo, H., Kobayashi, S., Ota, Y., et al. (2016). The JRA-55 Reanalysis: representation of atmospheric circulation and climate variability. *J. Meteor. Soc. Japan* 94, 269–302, doi: 10.2151/jmsj.2016-015

Hare, S. R., and Francis, R. C. (1995). Climate change and salmon production in the Northeast Pacific Ocean. *Can. Spec. Publ. Fish. Aquat. Sci. y* 121, 357–372.

Hersbach, H., Peubey, C., Simmons, A., Berrisford, P., Poli, P., and Dee, D. (2015). ERA- 20CM: a twentieth-century atmospheric model ensemble. *Q. J. R. Meteorol. Soc.* 141, 2350–2375. doi: 10.1002/qj.2528

Horel, J. D. (1981). A rotated principal component analysis of the interannual variability of the Northern Hemisphere 500 mb height field. *Monthly Weather Rev.* 109, 2080–2092.

Hoskins, B. J., and Ambrizzi, T. (1993). Rossby wave propagation on a realistic longitudinally varying flow. *J. Atmos. Sci.* 50, 1661–1671.

Hoskins, B. J., and Karoly, D. J. (1981). The steady linear response of a spherical atmosphere to thermal and orographic forcing. *J. Atmos. Sci.* 38, 1179–1196.

Huffman, G. J., Adler, R. F., Bolvin, D. T., Gu, G., Nelkin, E. J., and Wolff, D. B. (2007). The TRMM Multisatellite Precipitation Analysis (TMPA): quasi-global, multiyear, combined-sensor precipitation estimates at fine scales. *J. Hydrometeor.* 8, 38–55. doi: 10.1175/JHM560.1

Irving, D., and Simmonds, I. (2016). A new method for identifying the Pacific?South American pattern and its influence on regional climate variability. *J. Clim.* 29, 6109–6125. doi: 10.1175/JCLI-D-15-0843.1

Kalnay, E., Kanamitsu, M., Kistler, R., Collins, W., Deaven, D., Gandin, L., et al. (1996). The NCEP/NCAR 40-year reanalysis project. *Bull. Am. Meteorol. Soc.* 77, 437–471.

Karoly, D. J. (1989). Southern hemisphere circulation features associated with El Niño- Southern Oscillation events. *J. Clim.* 2, 1239–1252.

Kayano, M. T., and Andreoli, R. V. (2004). Decadal variability of northern northeast Brazil rainfall and its relation to tropical sea surface temperature and global sea level pressure anomalies. *J. Geophys. Res.* 109. doi: 10.1029/2004JC002429

Kidson, J. W. (1999). Principal modes of Southern Hemisphere low-frequency variability obtained from NCEP-NCAR reanalyses. *J. Clim.* 12, 2808–2830.

Kobayashi, S., Ota, Y., Harada, Y., Ebita, A., Moriya, M., Onoda, H., et al. (2015). The JRA-55 reanalysis: general specifications and basic characteristics. *J. Meteorol. Soc. Japan II* 93, 5–48. doi: 10.2151/jmsj.2015-001

Krishnamurthy, L., and Krishnamurthy, V. (2014). Influence of PDO on South Asian summer monsoon and monsoon–ENSO relation. *Clim. Dyn.* 42, 2397–2410. doi: 10.1007/s00382-013-1856-z

Latif, M., and Barnett, T. P. (1994). Causes of decadal climate variability over the North Pacific and North America. *Science* 266, 634–637. doi: 10.1126/science.266.5185.634

Latif, M., and Barnett, T. P. (1996). Decadal climate variability over the North Pacific and North America: dynamics and predictability. *J. Clim.* 9, 2407–2423.

Mantua, N. J., and Hare, S. R. (2002). The Pacific decadal oscillation. *J. Oceanogr.* 58, 35–44. doi: 10.1023/A:1015820616384

Mantua, N. J., Hare, S. R., Zhang, Y., Wallace, J. M., and Francis, R. C. (1997). A Pacific interdecadal climate oscillation with impacts on salmon production. *Bull. Am. Meteorol. Soc.* 78, 1069–1079.

Marengo, J. A., Soares, W. R., Saulo, C., and Nicolini, M. (2004). Climatology of the low-level jet east of the Andes as derived from the NCEP–NCAR reanalyses: characteristics and temporal variability. *J. Clim.* 17, 2261–2280. doi: 10.1175/1520-0442(2004)017<2261:COTLJE>2.0.CO;2

Minobe, S. (1997). A 50–70 year climatic oscillation over the North Pacific and *North* America. *Geophys. Res. Lett.* 24, 683–686. doi: 10.1029/97GL00504

Mo, K. C. (2000). Relationships between low-frequency variability in the Southern Hemisphere and sea surface temperature anomalies. *J. Clim.* 13, 3599–3610. doi: 10.1175/1520-0442(2000)013<3599:RBLFVI>2.0.CO;2

Mo, K. C., and Ghil, M. (1987). Statistics and dynamics of persistent anomalies. *J. Atmos. Sci.* 44, 877–902.

Mo, K. C., and Higgins, R. W. (1998). Tropical convection and precipitation regimes in the western United States. *J. Clim.* 11, 2404–2423.

Mo, K. C., and Paegle, J. N. (2001). The Pacific–South American modes and their downstream effects. *Int. J. Climatol.* 21, 1211–1229. doi: 10.1002/joc.685

Mo, K. C., and White, G. H. (1985). Teleconnections in the southern hemisphere. *Monthly Weather Rev.* 113, 22–37.

Mochizuki, T., Ishii, M., Kimoto, M., Chikamoto, Y., Watanabe, M., Nozawa, T., et al. (2010). Pacific decadal oscillation hindcasts relevant to near-term climate prediction. *Proc. Natl. Acad. Sci. U.S.A.* 107, 1833–1837. doi: 10.1073/pnas.0906531107

Nicolas, J. P., and Bromwich, D. H. (2014). New reconstruction of antarctic near-surface temperatures: multidecadal trends and reliability of global reanalyses*,+. *J. Clim.* 27, 8070–8093. doi: 10.1175/JCLI-D-13-00733.1

Poli, P., Hersbach, H., Dee, D. P., Berrisford, P., Simmons, A. J., Vitart, F., et al. (2016). ERA-20C: an atmospheric reanalysis of the twentieth century. *J. Clim.* 29, 4083–4097. doi: 10.1175/JCLI-D-15-0556.1

Poli, P., Hersbach, H., Tan, D., Dee, D., Thepaut, J. N., Simmons, A., et al. (2013). The data assimilation system and initial performance evaluation of the ECMWF pilot reanalysis of the 20th-century assimilating surface observations only (ERA-20C).

Renwick, J. A., and Revell, M. J. (1999). Blocking over the South Pacific and Rossby wave propagation. *Monthly Weather Rev.* 127, 2233–2247.

Rienecker, M. M., Suarez, M. J., Gelaro, R., Todling, R., Bacmeister, J., Liu, E., et al. (2011). MERRA: NASA's modern-era retrospective analysis for research and applications. *J. Clim.* 24, 3624–3648. doi: 10.1175/JCLI-D-11-00015.1

Robertson, A. W., and Mechoso, C. R. (2000). Interannual and interdecadal variability of the South Atlantic convergence zone. *Monthly Weather Rev.* 128, 2947–2957. doi: 10.1175/1520-0493(2000)128<2947:IAIVOT>2.0.CO;2

Schneider, U., Fuchs, T., Meyer-Christoffer, A., and Rudolf, B. (2008). *Produtos Globais de Análise de Precipitacão do GPCC*. Centro Global de Climatologia por Precipitação (GPCC), DWD, Internet Publication, 112.

Silva, C. B., Silva, M. E. S., and Ambrizzi, T. (2016). Climatic variability of river outflow in the Pantanal region and the influence of sea surface temperature. *Theor. Appl. Climatol.* 129, 97–109. doi: 10.1007/s00704-016-1760-7

Taylor, K. E., Stouffer, R. J., and Meehl, G. A. (2012). An overview of CMIP5 and the experiment design. *Bull. Am. Meteorol. Soc.* 93, 485–498. doi: 10.1175/BAMS-D-11-00094.1

Uppala, S. M., Kållberg, P. W., Simmons, A. J., Andrae, U., Bechtold, V. D. C., Fiorino, M. et al. (2005). The ERA-40 re-analysis. *Q. J. Roy. Meteor. Soc.*, 131, 2961–3012.

Villamayor, J., Ambrizzi, T., and Mohino, E. (2018). Influence of decadal sea surface temperature variability on northern Brazil rainfall in CMIP5 simulations. *Clim. Dyn.* 51, 563–579. doi: 10.1007/s00382-017-3941-1

Walker, G. T., and Bliss, E. W. (1932). World weather. V. *Mem. R. Meteor. Soc.* 4, 53–84.

Wallace, J. M., and Gutzler, D. S. (1981). Teleconnections in the geopotential height field during the Northern Hemisphere winter. *Monthly Weather Rev.* 109, 784–812.

Zamboni, L., Kucharski, F., and Mechoso, C. R. (2012). Seasonal variations of the links between the interannual variability of South America and the South Pacific. *Clim. Dyn.* 38, 2115–2129. doi: 10.1007/s00382-011-1116-z

Zhang, Y., Wallace, J. M., and Battisti, D. S. (1997). ENSO-like interdecadal variability: 1900-93. *J. Clim.* 10, 1004–1020.

Conflict of Interest: The authors declare that the research was conducted in the absence of any commercial or financial relationships that could be construed as a potential conflict of interest.